International Journal of Nanomedicine

Dovepress
Taylor & Francis Group

Open Access Full Text Article

ORIGINAL RESEARCH

Co-Delivery of Chemotherapy and Anti-Angiogenic Lipid via DPPA-LNPs Potentiates Anti-PD-1 Immunotherapy

Jiabao Tan[1–3,*], Junyue Fang[1,2,4,*], Wanrong Luo[1,2,5,*], Xiaojiang Chen[6], Yixia Liang[1,2], Ziqi Huang[1,2], Shiyu Tan[1,2], Meng Ren[3], Xiaoding Xu[1,2], Wenyue Zhang[1,2,5], Phei Er Saw[1,2]

[1]Guangdong Provincial Key Laboratory of Malignant Tumor Epigenetics and Gene Regulation, Medical Research Center, Sun Yat-Sen Memorial Hospital, Sun Yat-Sen University, Guangzhou, 510120, People's Republic of China; [2]Nanhai Translational Innovation Center of Precision Immunology, Sun Yat-Sen Memorial Hospital, Foshan, 528200, People's Republic of China; [3]Department of Endocrinology, Sun Yat-sen Memorial Hospital, Sun Yat-Sen University, Guangzhou, People's Republic of China; [4]Cellular and Molecular Diagnostics Center, Sun Yat-Sen Memorial Hospital, Sun Yat-Sen University, Guangzhou, 510120, People's Republic of China; [5]Department of Ultrasound, Sun Yat-Sen Memorial Hospital, Sun Yat-Sen University, Guangzhou, 510120, People's Republic of China; [6]Department of Gastric Surgery, Sun Yat-sen University Cancer Center; Sun Yat-sen University, Guangzhou, 510060, People's Republic of China

*These authors contributed equally to this work

Correspondence: Wenyue Zhang; Phei Er Saw, Email zhangwy226@mail.sysu.edu.cn; caipeie@mail.sysu.edu.cn

Background: Immune checkpoint inhibitor (ICI) therapies have marked a significant breakthrough in tumor immunotherapy. However, their clinical efficacy remains suboptimal in many cases. Emerging evidence indicates that resistance to ICIs is largely driven by the immunosuppressive nature of the tumor microenvironment (TME). Modulating the TME-through conventional chemotherapy or anti-angiogenic therapies has been shown to enhance immune activation and improve the therapeutic response to ICIs.

Methods: In this study, we developed epirubicin (EPI)-loaded lipid nanoparticles, termed DPPA(EPI) LNPs, which integrate the chemotherapeutic agent EPI with the anti-angiogenic lipid DPPA, enabling co-delivery and targeted enrichment within tumors. The cytotoxicity and anti-vascular endothelial cell tube formation properties of DPPA(EPI) LNPs were tested in vitro. The biosafety, anti-tumor ability and immunoactivities were tested on orthotopic tumor models of both breast cancer and hepatoma in vivo.

Results: DPPA(EPI) LNPs showed the advantages of uniformed particle size, high stability, good sustained-release effect. Compared to free drug, DPPA(EPI) LNPs significantly prolonged blood circulation (21.7% remaining at 12 h vs.16.5% at 30 min for free drug), enhanced tumor accumulation (18.4-fold change than free drug) and had well biological safety. In vivo, DPPA (EPI) LNPs showed excellent anti-tumor therapeutic efficacy by significantly inhibiting tumor cell proliferation (Ki67† cells reduced by 55%), reducing tumor angiogenesis (vascular density by 60%), and inducing stronger immunogenic cell death effect both in 4T1 orthotopic tumor model and Hepa1-6 orthotopic tumor model. And the treatment of DPPA (EPI) LNPs combined with programmed cell death protein 1 (PD-1) inhibitor further improved the activation of anti-tumor immunity in the TME, which leads to more significant inhibition of the tumor growth.

Conclusion: This dual-function nanoplatform—combining chemotherapy and anti-angiogenic therapy—substantially improved the efficacy of PD-1 blockade in both breast cancer and hepatocellular carcinoma (HCC) models. These findings offer a promising strategy and experimental foundation for TME modulation and the advancement of combination immunotherapy.

Keywords: dipalmitoyl phosphatidic acid, DPPA, programmed cell death protein 1, PD-1, tumor microenvironment, TME, immunogenic cell death, ICD, anti-angiogenesis

Introduction

With the development of oncology theory, many options have been provided with better efficacy and higher patient acceptance, such as immunotherapy. Immune checkpoint blockade therapies have provided new breakthroughs for clinical tumor treatment.[1] By inhibiting the immune evasion function of tumor cells and activating the body's immune system to monitor and kill tumor cells, immune checkpoint inhibitors (ICIs) represented by programmed cell death

Received: 4 June 2025
Accepted: 22 October 2025
Published: 25 November 2025

protein 1 (PD-1) inhibitors bring new hope and are widely used in clinic.[2–4] However, the efficacy of ICI monotherapy remains limited, with a substantial proportion of patients either failing to respond initially or developing resistance over the course of treatment, ultimately resulting in a lack of sustained clinical benefit.[5] For example, although malignant melanoma demonstrates one of the highest response rates to ICI therapy, approximately 60–70% of patients fail to achieve an objective response to PD-1 monoclonal antibody treatment, and 20–30% experience tumor recurrence or progression following initial therapy.[6,7] In most malignant tumors, the response rate of ICIs monotherapy remains low, the objective response rates are 15% to 25%, and survival benefits are limited.[8,9] Consequently, enhancing the antitumor efficacy of ICIs has become critical areas of ongoing research and clinical interest.

The tumor microenvironment (TME), composed of tumor cells, immune cells, stromal cells, and vasculature, plays a pivotal role in regulating tumor growth, metastasis, and colonization.[10] The American Association for Cancer Research (AACR) has identified key features and regulatory mechanisms underlying resistance to ICIs, including insufficient immunogenic tumor antigens, T cell dysfunction, a non-inflammatory tumor microenvironment, and aberrant genetic regulation,[11] inferring that TME is the key for regulating the efficacy of ICIs.[12] TME is typically characterized by hypoxia, accumulation of metabolic waste, acidic pH, and limited nutrient availability, which adversely impair the viability and activity of immune cells. Moreover, tumor cells actively recruit immune cells into the TME and manipulate them by inducing the expression of immune checkpoint molecules and secreting immunosuppressive cytokines, furtherly suppress immune cell function and contribute to the immunosuppressive TME.[13,14]

In TME, hypoxia and elevated metabolic activity stimulate the secretion of pro-angiogenic cytokines, thereby promoting neovascularization.[15–17] However, the newly formed vasculature is often structurally abnormal and functionally deficient, which exacerbates chemotherapy resistance, impairs immune cell infiltration and function, ultimately limits the efficacy of immunotherapy. Additionally, the dysfunctional vasculature facilitates tumor invasion and metastasis by providing favorable routes for tumor cell dissemination.[18,19] Several studies have reported that anti-angiogenic therapies can improve the perfusion in TME by normalizing aberrant vasculature, thereby facilitating immune cells infiltration and restoring or enhancing their function.[20–22] It is also reported that traditional chemotherapy not just only kills tumor cells directly, but also induces immunogenic cell death (ICD) of tumor cells which can release amounts of tumor immunogenic antigens and immune adjuvants to enhance the anti-tumor activity.[23,24] So, the combination of anti-angiogenic and chemotherapy therapy is hypothesized to exert a synergistic effect, jointly enhancing the therapeutic response to ICIs.

1,2-Dipalmitoyl-sn-glycero-3-phosphocholine (DPPA) is a naturally occurring anionic phospholipid and a secondary metabolite in the biosynthesis of glycerophospholipids. Recent research has demonstrated that DPPA can inhibit triple-negative breast cancer (TNBC) by downregulating cyclin B1 and inducing G2 phase cell cycle arrest.[25] Additionally, DPPA has been shown to suppress angiogenesis by inhibiting the CUX1/FGF1/HGF signaling pathway in endothelial cells.[26] In our previous works, we developed DPPA-based lipid nanoparticles (DPPA-LNPs) using a nanoprecipitation technique to overcome the hydrophobic limitations of DPPA. These nanoparticles exhibited improved stability, biosafety, and anti-angiogenic activity both in vitro and in vivo.[27] Furthermore, in incomplete radiofrequency ablation (IRFA) model of hepatocellular carcinoma (HCC), DPPA-LNPs were shown to downregulate the CUX1/FGF1 signaling pathway and reduce vascular endothelial growth factor A (VEGFA) expression in tumor cells. This dual action effectively suppressed neovascularization and inhibited the growth of residual tumors in IRFA-bearing mice.[28] However, the antitumor efficacy of DPPA-LNPs as a monotherapy remains limited. Therefore, leveraging DPPA-LNPs as a multifunctional drug delivery platform to encapsulate chemotherapeutic agents may enable the co-delivery of anti-angiogenic agents and chemotherapeutics, thereby maximizing therapeutic synergy and improving the efficacy of ICIs immunotherapy.

As a proof of concept, this study aims to design epirubicin (EPI)-loaded lipid nanoparticles (DPPA(EPI) LNPs), utilizing DPPA-LNPs as bioactive carriers for the co-delivery of the chemotherapeutic agent EPI (Scheme 1). Combined with PD-1 inhibitor, the therapeutic efficacy of this platform will be evaluated in breast cancer and HCC models. By leveraging the high tumor-targeting capability and enhanced accumulation offered by nanocarrier systems, this approach enables the simultaneous delivery of DPPA and EPI directly to tumor tissues. This strategy offers dual therapeutic benefits. First, the encapsulation of EPI within DPPA-LNPs improves its bioavailability, prolongs its cytotoxic activity against tumor cells, enhances the induction of ICD, and promotes antitumor immune activation within the TME. Second,

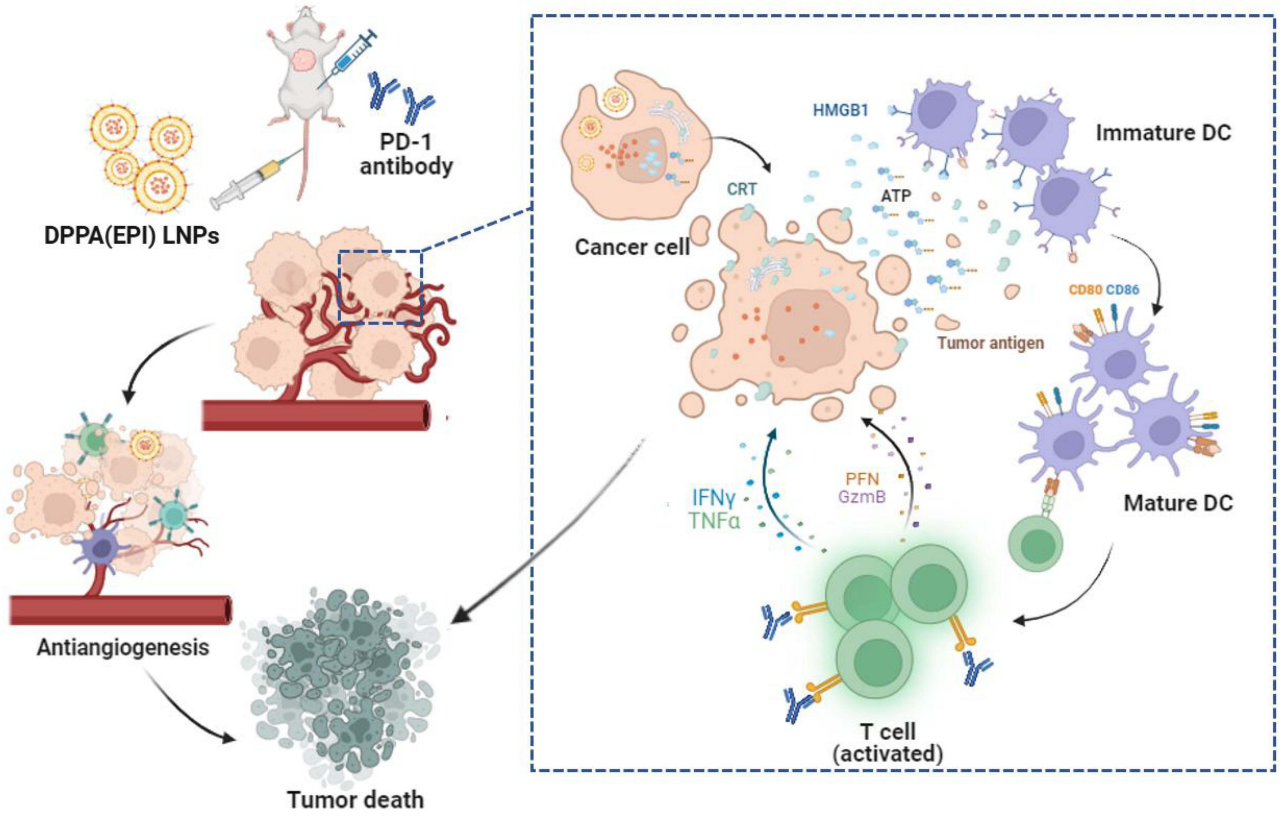

Scheme 1 Schematic illustration of the therapeutic effects of DPPA(EPI) LNPs on the activation of antitumor immunity and inhibition of angiogenesis to inhibit tumor growth.

DPPA contributes its anti-angiogenic properties by suppressing tumor neovascularization, reducing nutrient supply, improving perfusion within the TME, and facilitating immune cell infiltration and functional restoration. Collectively, DPPA (EPI) LNPs enable a synergistic combination of chemotherapy and anti-angiogenic therapy, amplifying antitumor immune responses and suppressing angiogenesis in the TME, which enhances anti-PD-1 immunotherapy. Our findings are expected to provide a novel strategy and experimental foundation for TME modulation and the development of next-generation combination therapies in cancer immunotherapy.

Methods

Material

1,2-dipalmitoyl-sn-glycero-3-phosphate (dipalmitoyl phosphatidic acid, DPPA), and DSPE-PEG 3400 were procured from Xi'an Rui Xi Biotechnology Co. (Xi'an, China). EPI and PD-1 inhibitor were purchased from Selleck. CD31 antibody and Calreticulin antibody were purchased from Proteintech Group (Wuhan, China), Ki67 antibody and CD8 antibody were purchased from Servicebio. HMGB1 antibody, Calreticulin antibody and Granzyme B antibody were purchased from Abcam. Perforin antibody, CD11c antibody and CD86 antibody were purchased from Cell Signal Technology. All other chemicals and reagents were of analytical grade and used in accordance with the manufacturer's instructions.

Synthesis and Characterization of DPPA(EPI) LNPs

DPPA(EPI) LNPs were prepared via the nanoprecipitation method as described in our previous publication. Briefly, a mixture of 10 μL EPI (2 mg/mL in methanol), 100 μL of DSPE-PEG3400 (10 mg/mL in methanol) and 400 μL of DPPA (5 mg/mL in methanol) were gradually added to 5 mL deionized water under continuous stirring for 3 min. This mixture was transferred to an Amicon filter (100 kDa) to eliminate methanol and any unbound substances. After centrifugation, the DPPA (EPI) LNPs

 https://doi.org/10.2147/IJN.S544668

would be retained in the upper chamber and be dispersed in 1 mL of PBS or deionized water. The size distribution of DPPA (EPI) LNPs was detected by dynamic light scattering method. The zeta potential was measured by Malvern nano-particle size potentiometer (MalvernzetasizerZSE, Malvern, UK). The morphology of DPPA LNPs was determined by 120 kV TEM.

Stability of DPPA(EPI) LNPs

After synthesis and purification, DPPA (EPI) LNPs were re-suspended in cultural medium containing 10% Fetal Bovine Serum (FBS) at 37 °C and PBS at room temperature. At pre-determined time point (15 min, 30 min, 1 h, 2 h, 4 h, 8 h, 12 h, 24 h and 48 h), the average particle size and distribution of DPPA(EPI) LNPs at each time point were detected by dynamic light scattering method.

Release of DPPA(EPI) LNPs

Release of DPPA(EPI) LNPs could be determined by the fluorescence intensity change of the EPI. The prepared nanoparticles were dispersed in 1 mL PBS and 1 mL complete medium transferred to a Float-a-lyzerG2 dialysis column with a molecular weight cut-off of 100kDa, then the dialysis column was immersed in beakers containing 1 L room temperature PBS and 37 °C PBS, respectively, and stirred continuously at a speed of 150 rpm. At the pre-determined time point (0, 0.5, 1, 2, 4, 8, 12, 24 and 48 h), 5 μL of the nanoparticles solution was withdrawn and mixed with 200 μL of DMSO. The fluorescence intensity of EPI was detected by Synergy HT multi-mode microplate reader.

Cell Culture

The mouse-derived TNBC cell line 4T1, mouse-derived HCC cell line Hepa1−6[29] and HUVEC were obtained from FuHeng Biology (ATCC, Shanghai). The 4T1 cells were cultured in RPMI 1640 medium, the Hepa1-6 cells were cultured in high glucose DMEM medium, HUVECs were cultured in ECM medium. Both culture media were supplemented with 10% fetal bovine serum (FBS), penicillin (100 units mL^{-1}), and streptomycin (100 μg mL^{-1}). Cells were maintained in a humidified cell culture chamber with 5% CO_2 at 37 °C.

In vitro Cellular Uptake

4T1 and Hepa1-6 cell were plated in glass bottom cell culture dish. DPPA(EPI) LNPs were added to the complete medium after 24 h. After 4 h incubation, the samples were washed three times with PBS and fixed with 4% paraformaldehyde (PFA). The nuclei were stained with Hoechst 33342. The images of the samples were taken by ZEISS 800 CLSM.

In vitro Cytotoxicity

4T1 and Hepa1-6 cell were plated in 96-well plates at a density of 5,000 cells per well. After 24 h, the fresh medium was replaced, and the concentration gradient was set with the equivalent concentration of EPI. After 48 h of incubation, the cell viabilities were tested by CCK8. The survival rate of tumor cells was calculated by comparing the differences between each treatment group and the control group.

Cell Proliferation in vitro

4T1 cells or Hepa1-6 cells were plated in 6-well plate with a density of 30,000 cells per well. After 24 h, we set up the day as D0, and grouped the cells with PBS, free EPI, DPPA LNPs and DPPA(EPI) LNPs for 48 h, then changed into a complete medium and kept cultured. The cell viabilities were tested on the pre-determined time point (D0, D2, D4, D6, D8) by Alamarblue solution.

Detection of ATP, CRT and HMGB1 in vitro

4T1 cells or Hepa1-6 cells were plated in 6-well plate with a density of 80,000 cells per well. After 24 h, PBS, free EPI, DPPA LNPs and DPPA(EPI) LNPs in fresh complete medium was incubated with cells for 48 h. The cell supernatant of each group was collected and the concentration of ATP was detected using Enhanced ATP Assay Kit (Beyotime). The CRT exposure and the HMGB1 secretion were detected by cellular immunofluorescence.

Tube Formation Assay

HUVEC were plated in 24-well plate with solidified Matrigel at a density of 40,000 cells per well. The DPPA LNPs group was added with the equivalent concentration of 40 μg/mL. After 6 h, the medium was removed and HUVEC were stained with calcein solution. The tube formation was observed under fluorescence microscope and photographed.

Animals

Healthy male C57BL/6 mice and female BALB/c mice aged 4–6 weeks were procured from the Experimental Animal Center of Sun Yat-sen University. All animal experiments were conducted following the GB/T 35892–2018 Laboratory animal-Guideline for ethical review of animal welfare guidelines and regulations approved by the Institutional Animal Ethics Committee of the Laboratory Animal Center of Sun Yat-sen University (License number: AP20230096).

4T1 Orthotopic Tumor Model

The 4T1 orthotopic tumor model was established in 6-week-old female BALB/c mice. 4T1 cells 4 × 10^5 cells were resuspended in 150 μL of PBS and implanted in the second mammary pad of mice. Successful orthotopic tumors could be seen and palpated within 6 days.

Hepa1-6 Orthotopic Tumor Model

The Luc-expressing Hepa1-6 orthotopic tumor model was established in 6-week-old male C57BL/6 mice. Hepa1-6 cells were prepared in DMEM (10% FBS and 50% matrigel). Healthy male C57BL/6 mice were anesthetized, and the liver was exposed via a tunnel made with microscopic surgical scissors and forceps. Luc-expressing Hepa1-6 was injected into the liver at the density of 4 × 10^6 cells in 25 μL per mouse and then the abdominal cavity was closed. Successful orthotopic tumors could be detected by examining the average radiance of tumor sites using bioluminescence imaging. Prior to imaging, D-luciferin substrate was intraperitoneally injected at dose of 150 mg/kg and the mice were viewed using an IVIS Lumina III (PerkinElmer, USA) imaging system.

Pharmacokinetics

Six healthy 6-week-old BALB/c mice were randomly divided into two groups. Cy5 and DPPA (Cy5) LNPs were injected through tail vein with the same equivalent dosage. 10 μL orbital blood was collected at pre-determined timepoint of 0 min, 5 min, 15 min, 30 min, 1 h, 2 h, 4 h, 8 h, 12 h and 24 h respectively. The fluorescence intensity of Cy5 in blood was measured and the blood circulation half-life of the drug was calculated.

Biodistribution

Six 4T1-orthotopic tumor bearing mice were randomly divided into two groups. Free Cy5 and DPPA(Cy5) LNPs were intravenously injected, respectively. After injection, the mice were perfused with PBS for systemic and pulmonary circulation at 24 h. Then, the mice were sacrificed, and the tumor, heart, liver, spleen, lung, kidney and muscle were removed. The accumulation of Cy5 in each tissue was observed by IVIS.

Toxicity

Healthy 6-week-old BALB/c mice were randomly divided into eight groups according to the treatment plan (n = 3). After three daily injections, the serum will be collected 24 h post the last injection and assayed for the determination of clinical chemistry parameters, including blood urea nitrogen (BUN), creatinine, alanine aminotransferase (ALT), aspartate aminotransferase (AST), and creatine kinase-MB (CK-MB). The histopathology analysis of heart, lung, kidney, spleen and liver were tested via H&E staining to evaluate the side effects.

Inhibition of Orthotopic Tumor Growth

When the 4T1 orthotopic tumor volume reached 60–80mm^3, tumor-bearing mice were randomly divided into 8 groups (n = 5) and were given injections of the following: i) PBS; ii) PD-1 antibody; iii) EPI; iv) DPPA LNPs; v) DPPA(EPI) LNPs; vi) EPI +

PD-1 antibody; vii) DPPA LNPs + PD-1 antibody and viii) DPPA(EPI) LNPs + PD-1 antibody. The equivalent dose of administration was 1 mg/kg EPI and/or 5 mg/kg PD-1 antibody per mouse. The body weights of mice were recorded every 2 days, and the longest and shortest diameters of the tumor were measured. The tumor volume was calculated by the following formula: $V = W^2 \times L /2$ (W is the shortest diameter of the tumor, and L is the longest diameter of the tumor). The experiment is terminated when the tumor size reaches 2000 mm^3. At the experimental endpoint, all tumors were harvested and sectioned.

Hepa1-6 orthotopic tumor-bearing mice were randomly divided into 8 groups (n = 3) and received the treatment the same as above. The tumor growth was monitored at day 0, 7, and 14 using bioluminescence imaging system according to the method described above. The experiment is terminated when the tumor-bearing mice develop severe hepatic ascites and abdominal swelling. At the experimental endpoint, all the tumors were collected and sectioned.

Immunohistochemistry (IHC)

After the aforementioned treatments, the mice were sacrificed and the tumors were harvested and embedded in paraffin for tumor sections. The slices were heated at 60 °C for 1 h and deparaffinized with xylene (20 min), anhydrous ethanol (5 min), 95% ethanol (5 min), 85% ethanol (5 min), and 75% ethanol (5 min) before washed by ddH_2O. Following antigen retrieval with DAKO target retrieval solution at a temperature of 95 °C for 15 min, and after washing, the slides were treated with 3% hydrogen peroxide for 10 min to scavenge peroxidase. After blocking with blocking buffer (5% normal goat serum and 5% BSA in PBS) for 2 h, the slices were incubated with primary antibody at 4 °C overnight. After washing with PBS thrice, secondary antibody with peroxidase-conjugated polymer was incubated for 30 min at RT. After the final turn washing, the slices were stained with DAB substrate-chromogen solution followed by hematoxylin. The slices were mounted and viewed under optical microscope.

Immunofluorescence (IF)

4T1 and Hepa1-6 cell were plated in glass bottom cell culture dish at the density of 80,000 per dish. After treated with drug in complete medium for 48 h, cells were washed with PBS thrice before fixation with 4% paraformaldehyde for 10 min. Triton X-100 (0.1% in PBS) was used when necessary to permeabilize for 10 min. Then, the cells were blocked with blocking buffer (5% normal goat serum and 5% BSA in PBS) at room temperature for 1 h. Thereafter, primary antibody was added to incubate at 4 °C overnight. After washed thrice with PBS, the cells were stained with Cy5-linked secondary antibody and Hoechst 33342 and finally viewed under a fluorescence microscope (Zeiss LSM 800).

Tumors were harvested and embedded in paraffin for tumor sections. The slices were heated at 60 °C for 1 h and deparaffinized with xylene, then the slices were dehygrated in decreasing ethanol concentrations before washed by ddH_2O. Following antigen retrieval with DAKO target retrieval solution at a temperature of 95 °C for 15 min, and after washing, the slides were treated with 3% hydrogen peroxide for 10 min to scavenge peroxidase. After blocking with blocking buffer (5% normal goat serum and 5% BSA in PBS) for 2 h, the slices were incubated with primary antibody at 4 °C overnight. After washing with PBS thrice, secondary antibody was incubated following the protocol of multi-fluorescent staining kit (RecordBio). The slices were mounted and viewed under a fluorescence microscope (Zeiss LSM 800).

Statistical Analysis

GraphPad Prism software (GraphPad, San Diego, CA) version 8 was used to perform statistical analysis and generate graphs. Data are represented as mean ± standard deviation (SD). Statistical significance was determined between pairs of data using two-tailed Student's *t*-test and one-way ANOVA. A statistical test with a P-value <0.05 was considered statistically significant.

Result

Fabrication and Characterization of DPPA (EPI) LNPs

To achieve the combined effects of chemotherapy and anti-angiogenic therapy, a self-antiangiogenic nanoplatform—designated DPPA(EPI) LNPs—was developed using a nanoprecipitation method. The nanoparticle formulation consisted of an outer shell composed of DPPA and DSPE-PEG3400, with EPI encapsulated in the core (Figure 1A). Visually,

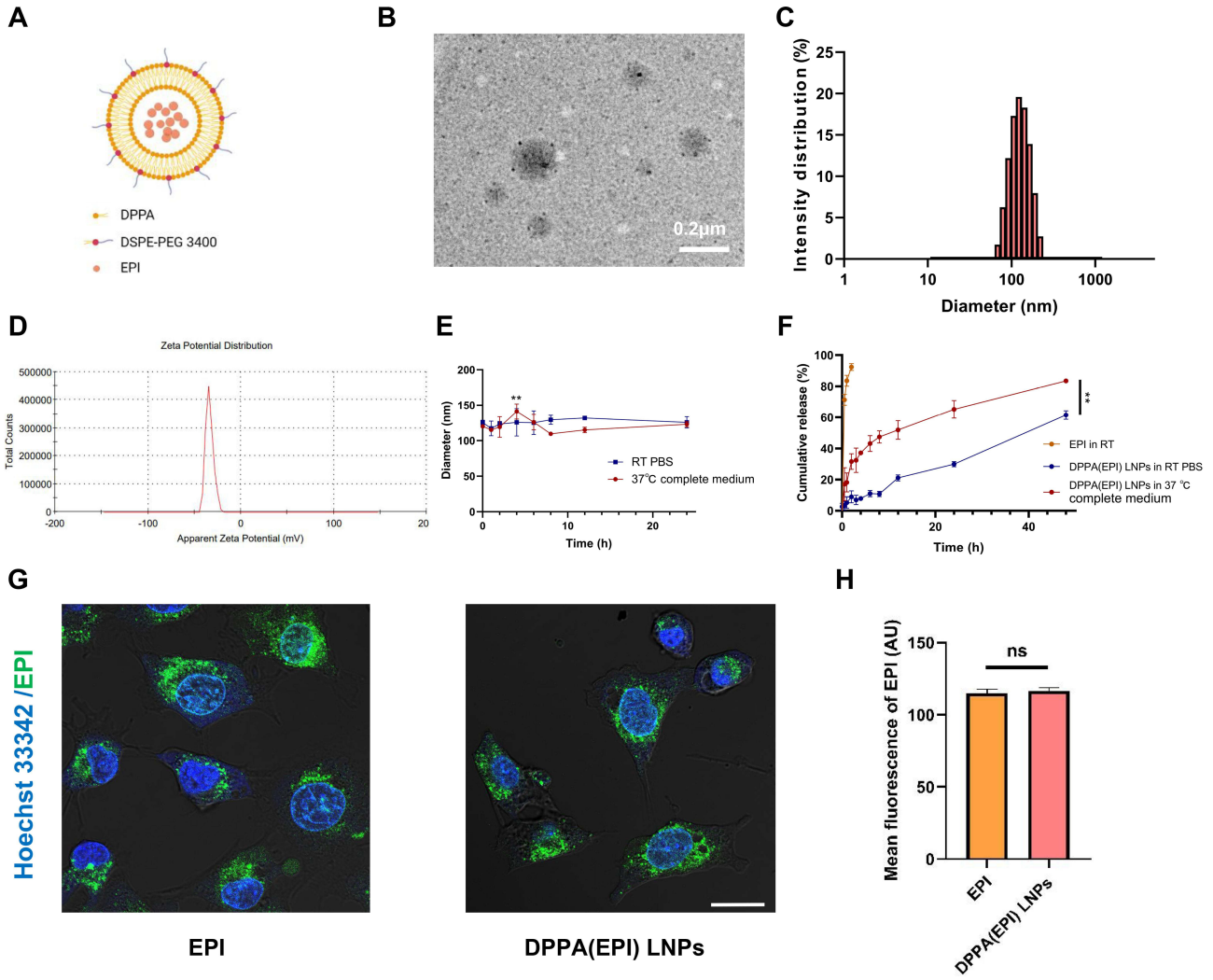

Figure 1 Characterization of DPPA(EPI) LNPs. The schematic structure (**A**), morphology (**B**), size (**C**), zeta potential (**D**), stability (**E**) and EPI release rate (**F**) of DPPA(EPI) LNPs (The scale bar indicated 200 nm). The confocal fluorescence imaging (**G**) and the quantitative analysis (**H**) of the uptake of EPI and DPPA(EPI) LNPs by 4T1 cells (The scale bar indicated 20 μm). (mean ± SD;**$p < 0.01$).

DPPA(EPI) LNPs appeared as orange, translucent suspensions that remained well-dispersed and stable in aqueous solutions such as water or PBS for extended periods, demonstrating improved solubility compared to free EPI dissolved in PBS. Transmission electron microscopy (TEM) revealed that the nanoparticles exhibited a uniform, spherical morphology with good dispersion (Figure 1B). Dynamic light scattering analysis indicated that the average particle diameter was 134.9 ± 2.59 nm, with a polydispersity index (PDI) of 0.25 ± 0.012, suggesting a relatively narrow size distribution (Figure 1C). The zeta potential measurement showed a negatively charged surface with a value of −34.0 ± 1.18 mV (Figure 1D), indicative of good colloidal stability. Fluorescence quantification assays confirmed that the encapsulation efficiency of EPI within the lipid nanoparticles was approximately 81.22%.

To evaluate the stability of DPPA(EPI) LNPs, the nanoparticles were dispersed in phosphate-buffered saline (PBS) at room temperature and in complete culture medium at 37 °C respectively (Figure 1E). In both environments, the particle size showed minor fluctuations within the first 4 hours—likely due to an initial release phase discussed below—but remained relatively stable over a 24-hour period. This indicates that DPPA(EPI) LNPs possess well stability. Drug release profiles further demonstrated the controlled release behavior of the nanoplatform. Free EPI exhibited rapid release, with 83.6 ± 3.50% of the drug released within the first hour at room temperature. In contrast, DPPA(EPI) LNPs showed a significantly slower release rate, with only 5.2 ± 3.68% released at room temperature and 18.2 ± 6.06% at 37 °C during

https://doi.org/10.2147/IJN.S544668

the same time period (Figure 1F). The release from DPPA(EPI) LNPs gradually increased over time: reaching 21.1 ± 1.95% within 12 hours at room temperature, and approximately 37.1 ± 1.25% within 4 hours at 37 °C, after which it plateaued. At the 48-hour time point, approximately 38.5% of the EPI remained in the nanoparticles at room temperature, and 16.5% at 37 °C. These findings demonstrated that DPPA(EPI) LNPs effectively prolonged the release of the encapsulated drug, offering a sustained release profile conducive to enhanced therapeutic performance.

The cellular uptake efficiency of DPPA(EPI) LNPs by tumor cells was also evaluated (Figure 1G and S1). Confocal fluorescence imaging demonstrated comparable intracellular accumulation between free EPI and DPPA(EPI) LNPs, indicating that nanoparticle encapsulation did not hinder EPI uptake by tumor cells (Figure 1G). Furthermore, fluorescence signals revealed that EPI delivered via DPPA(EPI) LNPs successfully localized to the nucleus within 4 hours, confirming effective intracellular release and nuclear transport of the drug (Figure 1H). These results suggested that DPPA(EPI) LNPs could efficiently deliver and release EPI into tumor cells.

The Anti-Tumor Effect of DPPA (EPI) LNPs in vitro

To evaluate the antitumor efficacy of DPPA(EPI) LNPs in vitro, both cytotoxicity and ICD induction were assessed using murine breast cancer 4T1 cells and murine HCC Hepa1-6 cells. Following 48 hours of incubation with increasing concentrations of EPI (equivalent doses), both free EPI and DPPA(EPI) LNPs exhibited comparable, dose-dependent inhibition of tumor cell viability (Figure 2A). Cell cycle analysis revealed that treatment with either EPI or DPPA(EPI) LNPs significantly reduced the proportion of cells in the S phase and increased the proportion of cells in the G2/M phase (Figure 2B and S2), indicating cell cycle arrest. There was no statistically significant difference between the two treatment groups ($p = 0.13$), suggesting that DPPA(EPI) LNPs maintain the antiproliferative activity of free EPI by effectively inducing G2/M phase arrest.

Apoptosis analysis by flow cytometry demonstrated that treatment with EPI and DPPA(EPI) LNPs resulted in comparable levels of tumor cell apoptosis. In 4T1 cells, the apoptotic rate was 43.57% in the EPI group and 42.84% in the DPPA(EPI) LNPs group (Figure 2C–E). Similarly, in Hepa1-6 cells, the apoptotic rates were 40.60% for EPI and 44.04% for DPPA(EPI) LNPs (Figure 2D–F). These results indicate that DPPA(EPI) LNPs effectively induce apoptosis in tumor cells, with no statistically significant difference compared to free EPI at equivalent doses. Proliferation assays further confirmed the antiproliferative effects of DPPA(EPI) LNPs. Compared with the control group, proliferation was significantly inhibited, with a reduction in fold expansion of 24.31 ± 1.79 in 4T1 cells and 27.29 ± 1.65 in Hepa1-6 cells (Figure 2G and H). Additionally, colony formation assays showed marked suppression of tumor cell clonogenicity. Both the number and size of colonies were significantly reduced in the DPPA(EPI) LNPs group compared to the control (Figure 2I and J). Taken together, DPPA(EPI) LNPs exhibit antitumor comparable activity to that of free EPI in inducing apoptosis, inhibiting proliferation and colony formation, highlighting their potential as an effective chemotherapeutic nanoplatform.

To further evaluate the ICD-inducing potential of DPPA(EPI) LNPs, three key ICD biomarkers-ATP release,[30] calreticulin (CRT) exposure,[31] and high mobility group box 1 (HMGB1) translocation[32,33] were assessed in 4T1 and Hepa1-6 cells. Treatment with DPPA(EPI) LNPs significantly increased extracellular ATP levels compared to the control group, with a 2.02 ± 0.223-fold increase in 4T1 cells and a 4.12 ± 0.752-fold increase in Hepa1-6 cells. These levels were comparable to those observed in the free EPI group (Figure 2K and L). Morphological observations revealed that tumor cells treated with either EPI or DPPA(EPI) LNPs exhibited characteristic swelling, accompanied by markedly increased CRT expression on the cell surface, indicating effective ICD induction (Figure 2M). In 4T1 cells, HMGB1 translocated from the nucleus to the cytoplasm following treatment with both formulations. While HMGB1 cytoplasmic translocation was less apparent in Hepa1-6 cells, a significant reduction in nuclear HMGB1 expression was observed. It was suggested that DPPA(EPI) LNPs effectively induced ICD in both tumor cell lines, demonstrating comparable activity to free EPI, confirming that DPPA(EPI) LNPs retain the immunostimulatory properties of EPI and have strong potential to enhance antitumor immune responses.

In vitro Antiangiogenic Effect of DPPA (EPI) LNPs

To assess whether the DPPA component within DPPA(EPI) LNPs retains anti-angiogenic activity, an in vitro angiogenesis assay was performed. At a DPPA-equivalent concentration of 40 μg/mL, both DPPA LNPs and DPPA(EPI) LNPs markedly disrupted tube formation of HUVECs (Figure 3A). Quantitative analysis revealed DPPA(EPI) LNPs

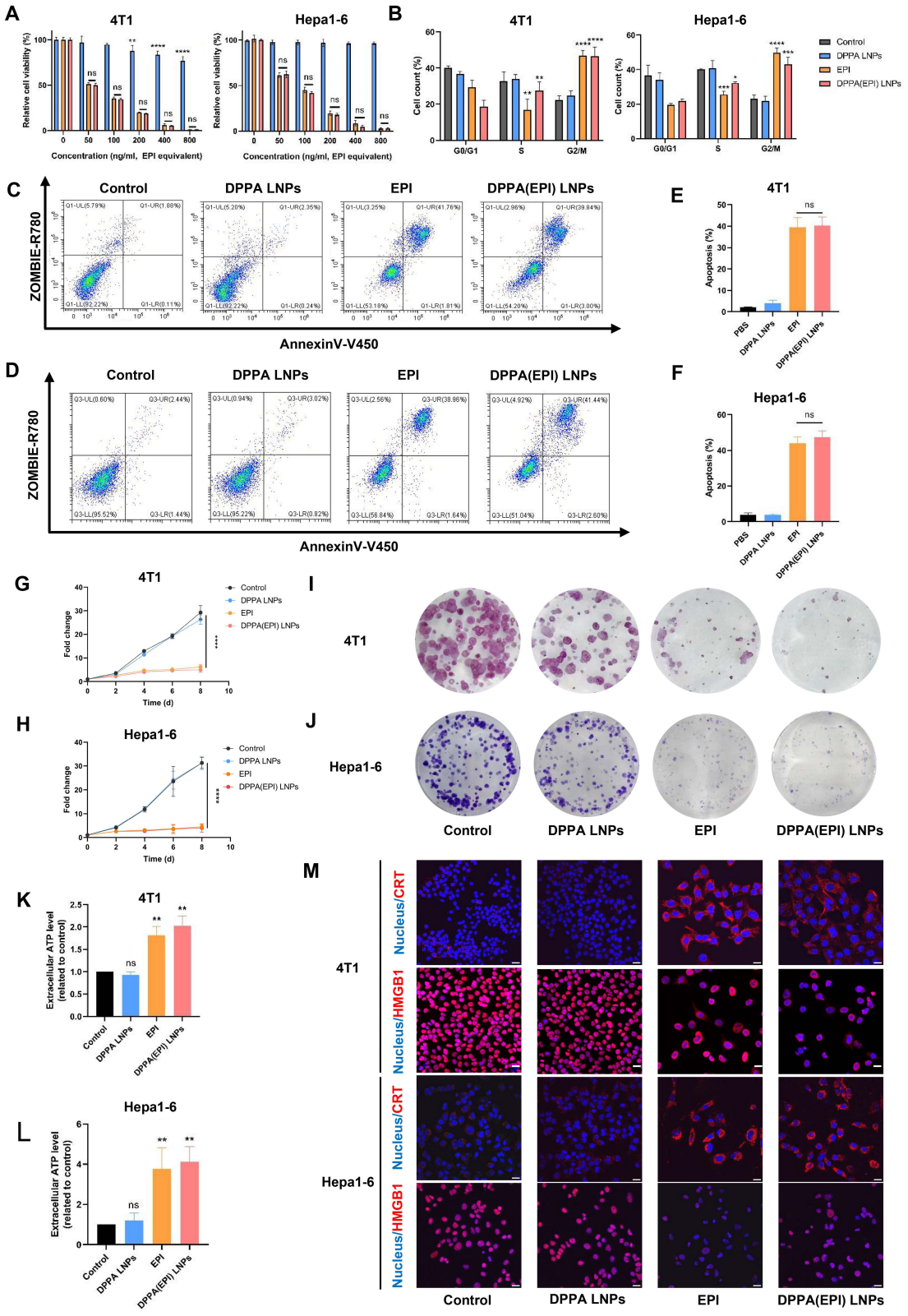

Figure 2 The anti-tumor effect of DPPA(EPI) LNPs in vitro. The cell viability of 4T1 cells and Hepa1-6 treated with DPPA(EPI) LNPs for 48 h (**A**). The statistical results of cell cycle of 4T1 cells and Hepa1-6 treated with DPPA(EPI) LNPs (**B**). The flowcytometry measurement and the statistical results of apoptosis of 4T1 cells (**C–E**) and Hepa1-6 cells (**D–F**) after treated with DPPA(EPI) LNPs. The growth curve of 4T1 cells (**G**) and Hepa1-6 (**H**) treated with DPPA(EPI) LNPs. The colony formation of 4T1 cells (**I**) and Hepa1-6 (**J**) treated with DPPA(EPI) LNPs. The increase of ATP in cellular supernatant of 4T1 (**K**) and Hepa1-6 (**L**). The fluorescence imaging detecting CRT and HMGB1 of 4T1 and Hepa1-6 after induced by DPPA(EPI) LNPs (**M**). (The scale bar indicated 20 μm; n = 3; mean ± SD; *$p < 0.05$; **$p < 0.01$; ***$p < 0.005$; ****$p < 0.001$).

https://doi.org/10.2147/IJN.S544668

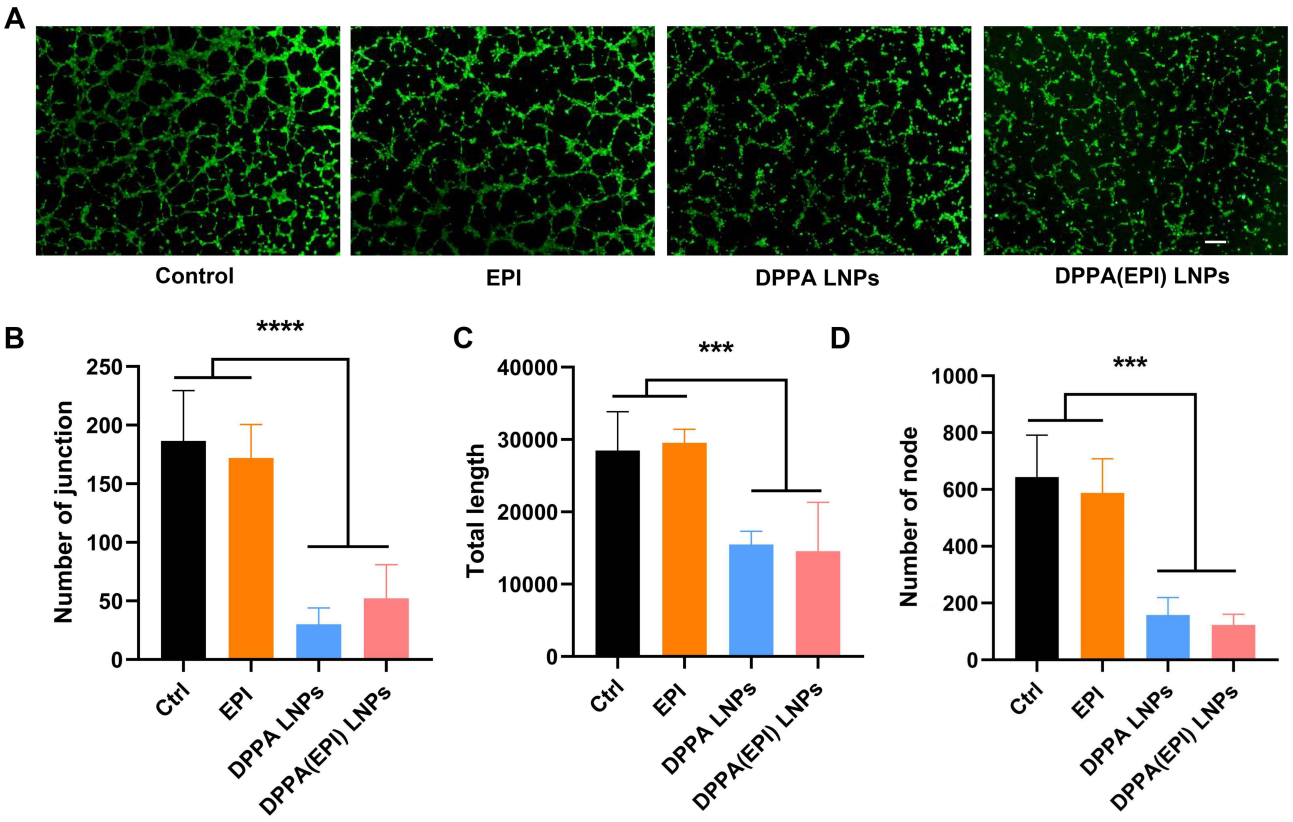

Figure 3 The anti-angiogenesis effect of DPPA(EPI) LNPs in vitro. Inhibition of HUVECs tube formation after treatment with DPPA(EPI) LNPs for 8 h (**A**). The statistical results of number of junction (**B**), total length (**C**) and number of node(**D**) in HUVECs tube formation experiment. (The scale bar indicated 100 μm; mean ± SD; ***$p < 0.005$; ****$p < 0.0001$).

significantly reduced the number of junctions, total tube length and nodes of HUVECs, compared to the control group (Figure 3B–D). These results indicated that DPPA(EPI) LNPs preserved the intrinsic anti-angiogenic properties and effectively inhibit endothelial cell-driven neovascularization in vitro.

The in vivo Anti-Tumor Effect of DPPA(EPI) LNPs in 4T1 Orthotopic Tumor Models

To further investigate the antitumor potential of DPPA(EPI) LNPs in vivo, key pharmacological properties—including pharmacokinetics, biodistribution, and biosafety—were first evaluated. Due to the overlap between EPI's fluorescence spectrum and blood autofluorescence, the hydrophobic fluorescent dye Cy5, which shares similar structural and molecular properties with EPI, was used as a surrogate tracer. As shown in Figure S3A, the free Cy5 monomer was rapidly cleared from circulation, with plasma levels dropping to 16.5 ± 9.30% within 30 minutes. In contrast, DPPA(Cy5) LNPs demonstrated prolonged circulation, maintaining approximately 42.9 ± 6.81% at 30 minutes, and gradually decreasing to 21.7 ± 5.81% at 12 hours. These results suggested that DPPA(EPI) LNPs significantly extended blood circulation time, likely due to the PEGylated lipid shell, enabling more sustained therapeutic drug levels. Fluorescence imaging of major organs and tumor tissues (Figure S3B and S3C) revealed that free Cy5 was primarily excreted via the kidneys, with fluorescence signals predominantly localized in renal tissues. In contrast, DPPA(Cy5) LNPs exhibited clear tumor enrichment, along with detectable distribution in major organs-a result consistent with extended circulation time and enhanced passive targeting. To assess biosafety, serum samples and major organs were collected following treatment. Hematoxylin and eosin (H&E) staining revealed no pathological abnormalities in the hearts, livers, spleens, lungs, or kidneys (Figure S4). Additionally, biochemical analysis of serum markers showed no signs of organ toxicity or systemic dysfunction (Figure S5). These findings confirm that DPPA(EPI) LNPs possessed favorable pharmacokinetic properties, efficient tumor targeting, and excellent biosafety, supporting their potential as a clinically viable drug delivery platform.

The in vivo antitumor efficacy of DPPA(EPI) LNPs and their synergistic potential when combined with PD-1 immune checkpoint blockade were evaluated. To establish 4T1 orthotopic breast cancer model, BALB/c mice were inoculated with 4T1 cells into the mammary fat pad, and treatments began once tumors reached an average volume of 80 mm^3. Mice were randomly assigned to eight groups (n = 5 per group) and treated as follows: G1: PBS (control), G2: PD-1 antibody (aPD-1), G3: free EPI, G4: DPPA LNPs, G5: DPPA(EPI) LNPs, G6: EPI + aPD-1, G7: DPPA LNPs + aPD-1, G8: DPPA(EPI) LNPs + aPD-1. DPPA(EPI) LNPs (EPI equivalent, 1 mg/kg) were administered via tail vein injection every other day for four doses, while aPD-1 (5 mg/kg) was given intraperitoneally every three days for a total of three doses (Figure 4A). After 18 days of treatment, mice were sacrificed for evaluation. Gross tumor images (Figure 4B), tumor volumes (Figure 4C), and tumor weights (Figure S6) were recorded. The results demonstrated that DPPA(EPI) LNPs significantly inhibited tumor growth in vivo, reducing tumor volume by approximately 80% compared to the PBS group and by about 65% compared to the free EPI group. Notably, DPPA LNPs alone also exhibited moderate antitumor effects, outperforming the EPI monotherapy group, suggesting that DPPA contributes additional therapeutic benefit beyond serving as a carrier. The combination treatment group (DPPA(EPI) LNPs + aPD-1) exhibited the most pronounced antitumor effect. Tumor volume in this group was reduced by an additional 70% compared to the DPPA(EPI) LNPs group alone. Importantly, the tumor growth remained suppressed even after treatment cessation, with tumor size increasing by less than 2-fold over the 10-day post-

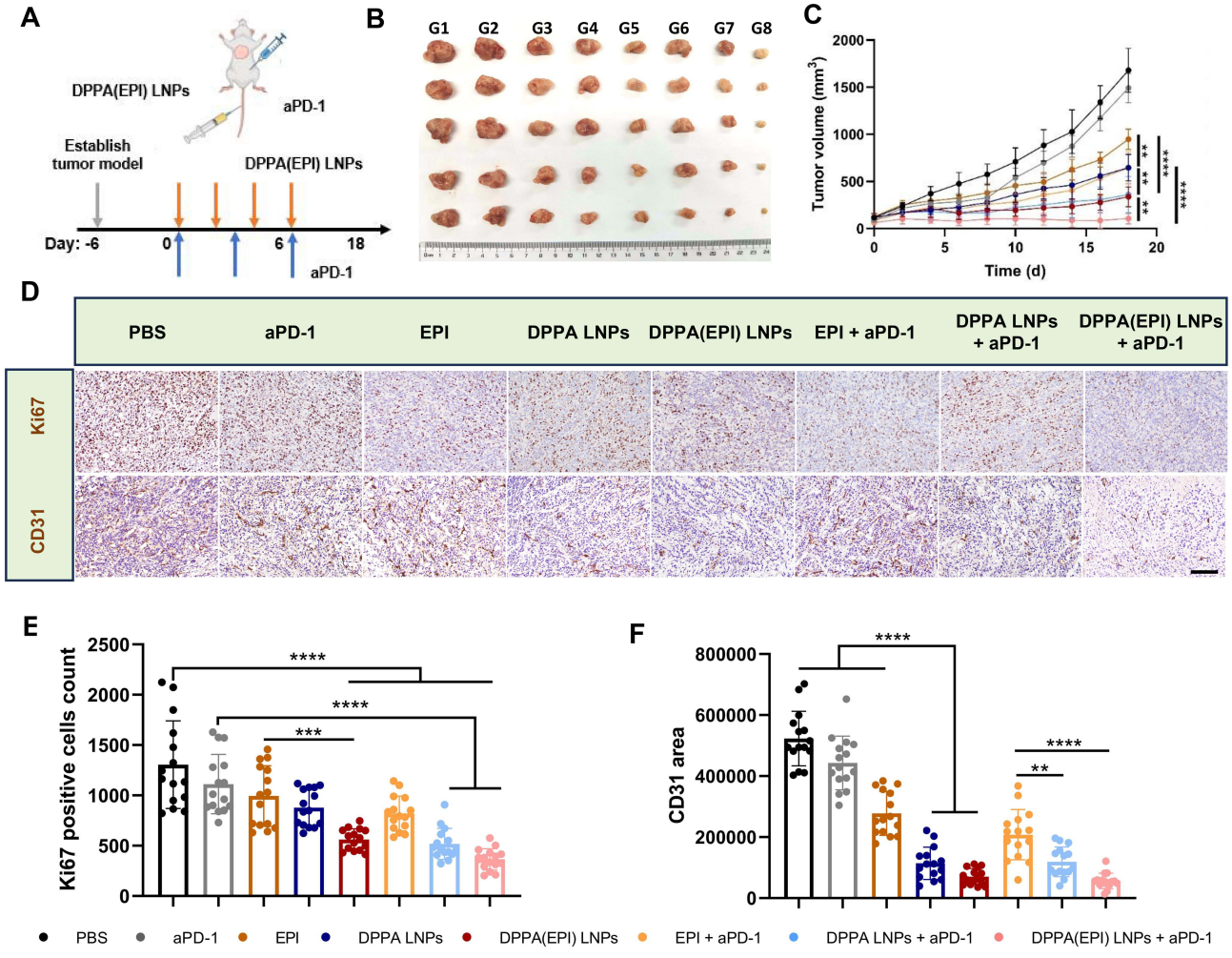

Figure 4 The in vivo anti-tumor effect of DPPA(EPI) LNPs in 4T1 orthotopic tumors. Experimental timeline and treatment schedule in each mouse for 4T1 orthotopic tumor-bearing mice (**A**). The gross image (**B**) and tumor growth curves (**C**) of 4T1 orthotopic tumors from each treatment group, and the groups were set as follows: G1: PBS, G2: PD-1 antibody (aPD-1), G3: free EPI (EPI), G4: DPPA LNPs, G5: DPPA(EPI) LNPs, G6: EPI combined with aPD-1 (EPI + aPD-1), G7: DPPA LNPs + aPD-1 and G8: DPPA(EPI) LNPs + aPD-1. The representative immunohistochemical image of proliferating cells (Ki67), tumor vessels (CD31) in each group (**D**). The statistical analysis of Ki67 (**E**) and CD31 (**F**) in each group. (The scale bar indicated 50 μm; n = 5; mean ± SD; $^{**}p<0.01$; $^{***}p<0.005$; $^{****}p<0.001$).

https://doi.org/10.2147/IJN.S544668

treatment observation period (D6–D16). Tumor weight measurements and anatomical observations were consistent with the tumor volume data (Figure S6). In summary, DPPA(EPI) LNPs demonstrated significant antitumor activity in the 4T1 breast cancer model, and this effect was further enhanced when combined with PD-1 immune checkpoint blockade, highlighting the therapeutic potential of this multifunctional nanoplatform for combination chemoimmunotherapy.

To assess the antitumor and anti-angiogenic effects of DPPA(EPI) LNPs in breast cancer, immunohistochemical staining for Ki67 (a proliferation marker) and CD31 (an endothelial cell marker) was performed on tumor tissue sections (Figure 4D). Compared to the PBS and EPI groups, DPPA(EPI) LNP treatment significantly reduced the number of Ki67† proliferating tumor cells. The combination treatment group (DPPA(EPI) LNPs + aPD-1) demonstrated the most pronounced reduction in Ki67 expression, indicating enhanced inhibition of tumor cell proliferation. These findings suggest that DPPA(EPI) LNPs not only exert strong antiproliferative effects but also synergize with PD-1 blockade to further enhance therapeutic efficacy (Figure 4E). CD31 staining revealed a marked decrease in microvessel density in tumors treated with DPPA-containing formulations. While some reduction in blood vessel density was also observed in the EPI and EPI + aPD-1 groups—likely due to the overall cytotoxic impact of EPI on the TME—treatment with DPPA(EPI) LNPs led to a more substantial decrease in tumor vasculature compared to either DPPA LNPs or EPI alone (Figure 4F). This confirms that DPPA retains its anti-angiogenic activity even when functioning as a drug carrier and works synergistically with EPI to suppress abnormal neovascularization. Collectively, these results validate that DPPA(EPI) LNPs effectively inhibit both tumor cell proliferation and angiogenesis, and further enhance the antitumor efficacy of PD-1 immune checkpoint inhibition.

The in vivo Anti-Tumor Effect of DPPA(EPI) LNPs in Hepa1-6 Orthotopic Tumor Models

To further evaluate the antitumor efficacy of DPPA(EPI) LNPs and their combinatorial effect with PD-1 blockade in HCC, we proved it on orthotopic Hepa1-6 tumor model. Tumor-bearing mice were randomly divided into eight groups (n = 3 per group) and treated as follows: G1: PBS (control), G2: PD-1 antibody (aPD-1), G3: free EPI (EPI), G4: DPPA LNPs, G5: DPPA(EPI) LNPs, G6: EPI + aPD-1, G7: DPPA LNPs + aPD-1, G8: DPPA(EPI) LNPs + aPD-1. DPPA(EPI) LNPs (EPI equivalent, 1 mg/kg) were administered via tail vein injection every other day for four total doses, while aPD-1 (5 mg/kg) was administered intraperitoneally every three days for three doses (Figure 5A). After 14 days of treatment, mice were sacrificed, and tumor burden was evaluated. The results demonstrated that DPPA(EPI) LNPs significantly inhibited tumor growth compared to all monotherapy groups and markedly enhanced the therapeutic efficacy of PD-1 blockade (Figure 5B and C). Immunohistochemical analysis of tumor tissues for Ki67 and CD31 (Figure 5D) revealed that DPPA(EPI) LNPs substantially reduced tumor cell proliferation and improved the responsiveness to aPD-1 treatment in the Hepa1-6 orthotopic tumor model (Figure 5E). Importantly, DPPA(EPI) LNPs also exhibited the strongest anti-angiogenic effect among all treatment groups, as evidenced by the most pronounced reduction in CD31-positive vasculature (Figure 5F). These results suggested that the dual action of DPPA(EPI) LNPs—combining chemotherapeutic and anti-angiogenic effects—not only directly inhibits tumor growth but also enhances immune-mediated tumor suppression when combined with PD-1 checkpoint blockade.

The Efficacy for Immune Activation of DPPA(EPI) LNPs in Orthotopic Tumor Models

The above results demonstrated that DPPA(EPI) LNPs exert potent antitumor and anti-angiogenic effects in both 4T1 and Hepa1-6 orthotopic tumor models. Our prior in vitro studies further confirmed that DPPA(EPI) LNPs induce ICD at levels comparable to free EPI. To assess the in vivo immunostimulatory potential of DPPA(EPI) LNPs and evaluate their ability to enhance immune activation in the context of PD-1 checkpoint blockade, we employed the same treatment regimens in orthotopic 4T1 and Hepa1-6 tumor-bearing mouse models. Mice were sacrificed on day 4 following treatment initiation for downstream immunological analysis (Figure 6A–F).

To verify ICD induction in vivo, CRTwas assessed via immunofluorescence staining of tumor tissues (Figure 6B–G). The DPPA(EPI) LNPs group showed significantly higher CRT expression compared to the free EPI group, indicating more effective induction of ICD. These findings suggested that nanoparticle encapsulation enhances EPI enrichment at the tumor site and amplifies ICD, which may contribute to heightened immune activation within the TME in vivo.

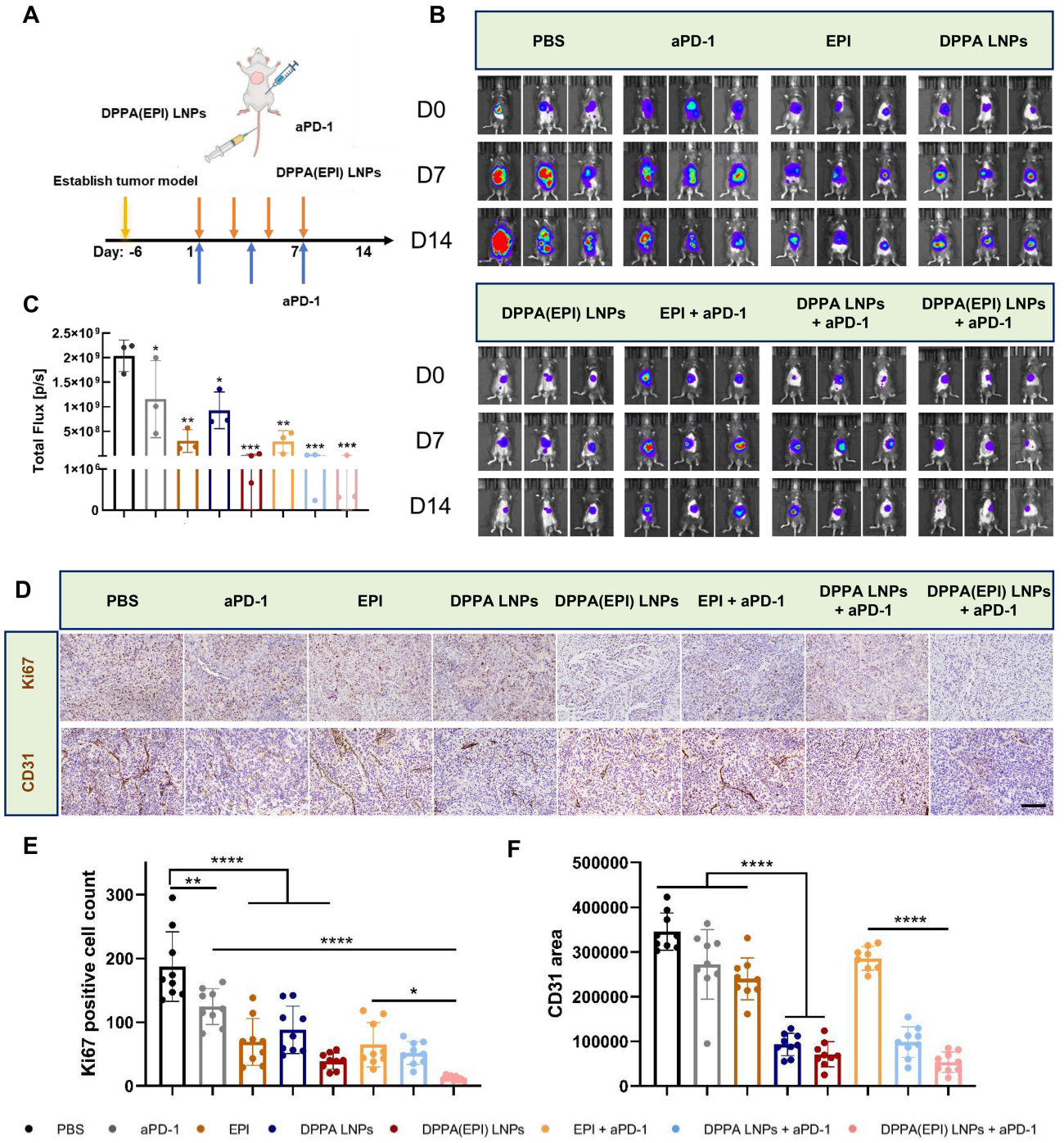

Figure 5 The in vivo anti-tumor effect of DPPA(EPI) LNPs in Hepa1-6 orthotopic tumors. The experimental timeline and treatment schedule in each mouse for Hepa1-6 orthotopic tumor-bearing mice (**A**). The bioluminescence images (**B**) and statistical result (**C**) of Hepa1-6 orthotopic tumors from each treatment group. The representative immunohistochemical image of proliferating cells (Ki67), tumor vessels (CD31) in each group (**D**). The statistical analysis of Ki67 (**E**) and CD31 (**F**) in each group. (The scale bar indicated 50 μm; n = 5; mean ± SD; * $p < 0.05$; ** $p < 0.01$; **** $p < 0.001$).

To further evaluate the ability of DPPA(EPI) LNPs to regulate antigen presentation within the TME, we assessed dendritic cell (DC) infiltration and maturation by detecting the DC surface marker CD11c and the co-stimulatory molecule CD86. As shown in Figure 6A and F, treatment with DPPA(EPI) LNPs significantly increased both the infiltration of CD11c† cells and the expression of CD86 within the TME. CD86, a ligand for CD28 on T cells, is a key marker of antigen-presenting cell (APC) activation and is essential for initiating effective CD8† T cell responses.

https://doi.org/10.2147/IJN.S544668

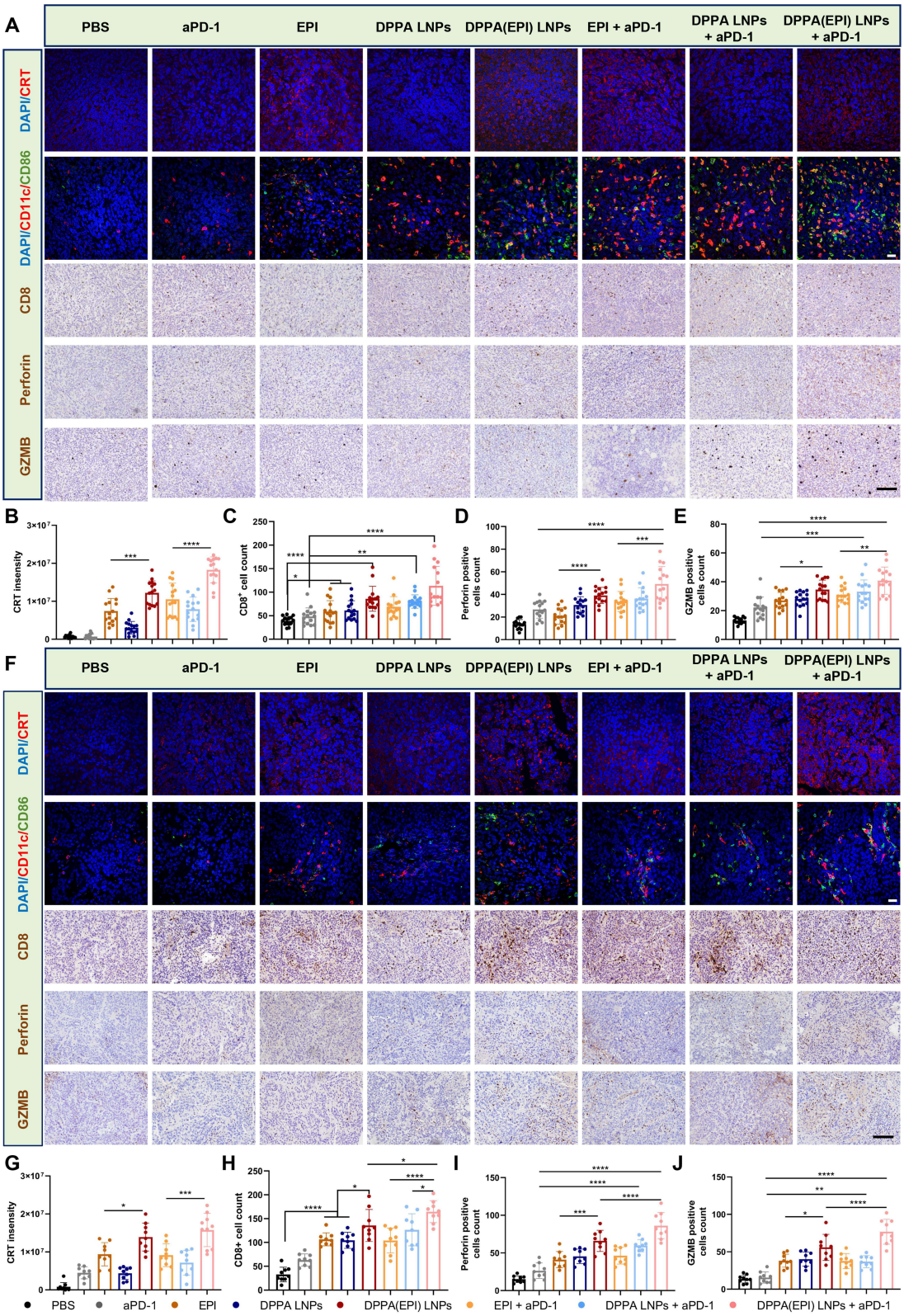

Figure 6 The in vivo immune-activation of DPPA(EPI) LNPs in orthotopic tumors. The representative image of CRT, DCs, CD8, Perforin and Granzyme B in each group of 4T1 orthotopic tumors (**A**). The statistic of CRT (**B**), CD8 (**C**), Perforin (**D**) and Granzyme B (**E**) in each group of 4T1 orthotopic tumors. The representative image of CRT, DCs, CD8, Perforin and Granzyme B in each group of Hepa1-6 orthotopic tumors (**F**). The statistic of CRT (**G**), CD8 (**H**), Perforin (**I**) and Granzyme B (**J**) in each group of 4T1 orthotopic tumors. (The scale bar indicated 50 μm in IHC image and 20 μm in IF image; 4T1 orthotopic tumors model n = 5; Hepa1-6 orthotopic tumors model n = 3; mean ± SD; *$p < 0.05$; **$p < 0.01$; ***$p < 0.005$; ****$p < 0.001$).

The elevated expression of CD86 suggests enhanced APC maturation and antigen presentation capacity, which is critical for T cell priming and improved responsiveness to PD-1 blockade therapy.

To investigate the adaptive immunity, we further analyzed CD8† T cell infiltration and effector function in tumor tissues. Compared to all monotherapy groups, the DPPA(EPI) LNPs treatment resulted in the highest levels of CD8† T cell infiltration (Figure 6C–H), along with significantly increased expression of perforin (Figure 6D–I) and granzyme B (Figure 6E–J)-both of which are cytolytic molecules critical for T cell-mediated tumor cell killing. These findings indicated that DPPA(EPI) LNPs not only promoted T cell recruitment but also enhanced their functional cytotoxicity.

In summary, DPPA(EPI) LNPs demonstrated superior performance in reducing tumor growth and angiogenesis, while simultaneously eliciting the most robust immune activation in both 4T1 and Hepa1-6 orthotopic tumor models. These synergistic effects within the TME translated into enhanced therapeutic efficacy when combined with PD-1 immune checkpoint inhibition, offering a promising strategy for nanomedicine-based combination immunotherapy.

Discussion

The development of DPPA(EPI) LNPs represents a pivotal advancement in combining chemotherapy with anti-angiogenic therapy within a single nanoplatform. DPPA, a bioactive lipid, not only serves as a structural component of the lipid nanoparticle but also inhibits tumor angiogenesis by downregulating the CUX1/FGF1/HGF signaling pathway in endothelial cells.[25–28] Concurrently, EPI is encapsulated to induce cytotoxicity and ICD. In vitro angiogenesis assays demonstrated that DPPA(EPI) LNPs significantly disrupted tube formation in HUVECs, reducing the number of junctions, total tube length, and nodes by 62%, 58%, and 71%, respectively, compared to the control group (all $p < 0.001$). This confirmed that DPPA retained its anti-angiogenic activity even when co-delivering EPI. In vivo, DPPA(EPI) LNPs exhibited prolonged blood circulation (42.9% remaining at 30 minutes vs 16.5% for free drug) and enhanced tumor accumulation, as shown by fluorescence imaging of Cy5-labeled nanoparticles. In the 4T1 breast cancer model, DPPA(EPI) LNPs reduced tumor vascular density (CD31† vessels) by 60% compared to PBS, while also suppressing tumor cell proliferation (Ki67† cells reduced by 55%). This dual mechanism of action—direct cytotoxicity via EPI and anti-angiogenic remodeling via DPPA—creates a synergistic effect that surpasses single-agent therapies.

A central challenge in immunotherapy is the immunosuppressive TME, which limits the efficacy of PD-1 blockade. DPPA (EPI) LNPs address this by inducing robust ICD, as evidenced by increased extracellular ATP release (2.02-fold in 4T1, 4.12-fold in Hepa1-6 cells) and cell surface calreticulin (CRT) exposure, comparable to free EPI but with prolonged effects due to sustained drug release.[30,31,33] This ICD profile promoted dendritic cell (DC) maturation, as shown by increased CD11c†CD86† cell infiltration in tumor tissues (1.8-fold increase in 4T1 model).[32] Furthermore, DPPA's anti-angiogenic activity normalized tumor vasculature, reducing hypoxia and interstitial fluid pressure. [34–36] This improvement facilitated CD8†T cell infiltration, with DPPA(EPI) LNPs + aPD-1 group showing a 2.3-fold increase in CD8† T cells compared to aPD-1 monotherapy in Hepa1-6 tumors. Concomitantly, the expression of cytotoxic molecules perforin and granzyme B was significantly upregulated ($p < 0.001$), indicating enhanced T cell effector function.

The combination of DPPA(EPI) LNPs with PD-1 inhibition yielded striking antitumor effects in both 4T1 and Hepa1-6 orthotopic models. In 4T1 tumors, the dual therapy reduced tumor volume by 92% compared to PBS, outperforming DPPA(EPI) LNPs alone (80% reduction) or aPD-1 alone (35% reduction). This synergy stems from three interconnected mechanisms: (1) EPI-induced ICD provides tumor antigens and DAMPs to prime adaptive immunity; (2) DPPA normalizes vasculature to improve immune cell access; and (3) PD-1 blockade reinvigorates exhausted T cells within the reprogrammed TME.[8,12] Notably, in the Hepa1-6 model, DPPA(EPI) LNPs + aPD-1 suppressed tumor growth by 85% compared to the control, with minimal toxicity observed in major organs (H&E staining showed no pathological abnormalities). This contrasts with traditional anti-angiogenic agents like bevacizumab, which often exhibit systemic toxicity and limited TME-penetrating efficiency.[36]

DPPA(EPI) LNPs offer distinct advantages over conventional combination strategies: (1) Targeted co-delivery: The nanoplatform ensures concurrent release of EPI and DPPA at the tumor site, overcoming pharmacokinetic mismatches inherent in sequential drug administration;[37,38] (2) Reduced systemic toxicity: The PEGylated lipid shell minimizes off-tumor accumulation, as shown by negligible Cy5 fluorescence in non-tumor organs;[27] (3) Multifunctional design: The

lipid-based architecture allows for future modification with more inherent self-therapeutic bioactive materials, targeting ligands or imaging agents, enhancing translational potential for precision oncology.[29]

While this study demonstrates promising preclinical efficacy, several challenges warrant further investigation. First, the optimal dosing schedule for clinical translation requires validation, particularly in contexts of hepatic dysfunction given EPI's hepatotoxicity profile. Second, long-term resistance to anti-angiogenic therapy—such as vasculogenic mimicry—may necessitate combination with agents targeting alternative pathways (eg, MET, AXL).[39,40] Third, the temporal sequencing of chemotherapy and immunotherapy (eg, priming with DPPA(EPI) LNPs before aPD-1 administration) should be optimized to maximize immune activation.[36]

Conclusion

In this study, we successfully designed and developed DPPA(EPI) LNPs, a multifunctional lipid nanoparticle system capable of achieving the co-delivery and tumor-specific enrichment of both EPI and the bioactive lipid DPPA. DPPA(EPI) LNPs represent a transformative strategy to synergize chemotherapy, anti-angiogenesis, and immunotherapy by reprogramming the TME. By addressing multiple resistance mechanisms, this dual-function nanoplatform provides a robust foundation for developing next-generation combination therapies, offering new hope for improving PD-1 blockade efficacy in solid tumors.

Acknowledgments

This study was supported by the National Natural Science Foundation of China (82202162, 82171944), Natural Science Foundation of Guangdong Province (2025A1515010075), the Science and Technology Program of Guangzhou (2025A04J4442), Guangzhou bureau of basic science grant (202201020576), 111 project (No. B20056), Guangdong Basic and Applied Basic Research Foundation (2022A1515110065, 2024B1515040006), National Natural Science Foundation of China (82001822), Natural Science Foundation of Guangdong Province of China (2024A1515010091), Guangzhou Municipal Science and Technology Bureau (201704020131), the Guangdong Provincial Fund for Distinguished Young Scholars (2021B1515020066) and the "Three million for Three Years" Project of the High-level Talent Special Funding Scheme of Sun Yat-Sen Memorial Hospital (132090023).

Disclosure

The authors report no conflicts of interest in this work.

References

1. Wang Y, Gao D, Liu Y, et al. Immunogenic-cell-killing and immunosuppression-inhibiting nanomedicine. *Bioact Mater*. 2021;6(6):1513–1527. doi:10.1016/j.bioactmat.2020.11.016
2. Chen L, Flies DB. Molecular mechanisms of T cell co-stimulation and co-inhibition. *Nat Rev Immunol*. 2013;13(4):227–242. doi:10.1038/nri3405
3. Willimsky G, Blankenstein T. Sporadic immunogenic tumours avoid destruction by inducing T-cell tolerance. *Nature*. 2005;437(7055):141–146. doi:10.1038/nature03954
4. Keir ME, Butte MJ, Freeman GJ, Sharpe AH. PD-1 and its ligands in tolerance and immunity. *Annu Rev Immunol*. 2008;26(1):677–704. doi:10.1146/annurev.immunol.26.021607.090331
5. de Miguel M, Calvo E. Clinical Challenges of Immune Checkpoint Inhibitors. *Cancer Cell*. 2020;38(3):326–333. doi:10.1016/j.ccell.2020.07.004
6. Ott PA, Bang YJ, Piha-Paul SA, et al. T-cell-inflamed gene-expression profile, programmed death ligand 1 expression, and tumor mutational burden predict efficacy in patients treated with pembrolizumab across 20 cancers: KEYNOTE-028. *J Clin Oncol*. 2019;37(4):318–327. doi:10.1200/JCO.2018.78.2276
7. Garon EB, Rizvi NA, Hui R, et al. Pembrolizumab for the treatment of non-small-cell lung cancer. *N Engl J Med*. 2015;372(21):2018–2028. doi:10.1056/NEJMoa1501824
8. Bagchi S, Yuan R, Engleman EG. Immune checkpoint inhibitors for the treatment of cancer: clinical impact and mechanisms of response and resistance. *Annu Rev Pathol*. 2021;16(1):223–249. doi:10.1146/annurev-pathol-042020-042741
9. Bellmunt J, de Wit R, Vaughn DJ, et al. Pembrolizumab as second-line therapy for advanced urothelial carcinoma. *N Engl J Med*. 2017;376(11):1015–1026. doi:10.1056/NEJMoa1613683
10. de Visser KE, Joyce JA. The evolving tumor microenvironment: from cancer initiation to metastatic outgrowth. *Cancer Cell*. 2023;41(3):374–403. doi:10.1016/j.ccell.2023.02.016
11. Karasarides M, Cogdill AP, Robbins PB, et al. Hallmarks of resistance to immune-checkpoint inhibitors. *Cancer Immunol Res*. 2022;10(4):372–383. doi:10.1158/2326-6066.CIR-20-0586
12. Bejarano L, Jordão MJC, Joyce JA. Therapeutic targeting of the tumor microenvironment. *Cancer Discov*. 2021;11(4):933–959. doi:10.1158/2159-8290.CD-20-1808
13. Gajewski TF, Schreiber H, Fu YX. Innate and adaptive immune cells in the tumor microenvironment. *Nat Immunol*. 2013;14(10):1014–1022. doi:10.1038/ni.2703

14. Tang T, Huang X, Zhang G, Hong Z, Bai X, Liang T. Advantages of targeting the tumor immune microenvironment over blocking immune checkpoint in cancer immunotherapy. *Signal Transduct Target Ther*. 2021;6(1):72. doi:10.1038/s41392-020-00449-4
15. De Palma M, Biziato D, Petrova TV. Microenvironmental regulation of tumour angiogenesis. *Nat Rev Cancer*. 2017;17(8):457–474. doi:10.1038/nrc.2017.51
16. Klein D. The tumor vascular endothelium as decision maker in cancer therapy. *Front Oncol*. 2018;8:367. doi:10.3389/fonc.2018.00367
17. Harrell CR, Markovic BS, Fellabaum C, Arsenijevic A, Djonov V, Volarevic V. Molecular mechanisms underlying therapeutic potential of pericytes. *J Biomed Sci*. 2018;25(1):21. doi:10.1186/s12929-018-0423-7
18. Sormendi S, Wielockx B. Hypoxia pathway proteins as central mediators of metabolism in the tumor cells and their microenvironment. *Front Immunol*. 2018;9:40. doi:10.3389/fimmu.2018.00040
19. Jiang X, Wang J, Deng X, et al. The role of microenvironment in tumor angiogenesis. *J Exp Clin Cancer Res*. 2020;39(1):204. doi:10.1186/s13046-020-01709-5
20. Greten TF, Villanueva A, Korangy F, et al. Biomarkers for immunotherapy of hepatocellular carcinoma. *Nat Rev Clin Oncol*. 2023;20(11):780–798. doi:10.1038/s41571-023-00816-4
21. Finn RS, Qin S, Ikeda M, et al. Atezolizumab plus bevacizumab in unresectable hepatocellular carcinoma. *N Engl J Med*. 2020;382(20):1894–1905. doi:10.1056/NEJMoa1915745
22. Makker V, Rasco D, Vogelzang NJ, et al. Lenvatinib plus pembrolizumab in patients with advanced endometrial cancer: an interim analysis of a multicentre, open-label, single-arm, Phase 2 trial. *Lancet Oncol*. 2019;20(5):711–718. doi:10.1016/S1470-2045(19)30020-8
23. Sun Q, Hong Z, Zhang C, Wang L, Han Z, Ma D. Immune checkpoint therapy for solid tumours: clinical dilemmas and future trends. *Signal Transduct Target Ther*. 2023;8(1):320.
24. Yi M, Zheng X, Niu M, Zhu S, Ge H, Wu K. Combination strategies with PD-1/PD-L1 blockade: current advances and future directions. *Mol Cancer*. 2022;21(1):28. doi:10.1186/s12943-021-01489-2
25. Chen J, Zhou Z, Yao Y, et al. Dipalmitoylphosphatidic acid inhibits breast cancer growth by suppressing angiogenesis via inhibition of the CUX1/FGF1/HGF signalling pathway. *J Cell Mol Med*. 2018;22(10):4760–4770. doi:10.1111/jcmm.13727
26. Zhang QQ, Chen J, Zhou DL, et al. Dipalmitoylphosphatidic acid inhibits tumor growth in triple-negative breast cancer. *Int J Biol Sci*. 2017;13(4):471–479. doi:10.7150/ijbs.16290
27. Cao S, Zhang W, Pan H, et al. Bioactive lipid-nanoparticles with inherent self-therapeutic and anti-angiogenic properties for cancer therapy. *Acta Biomater*. 2023;157:500–510. doi:10.1016/j.actbio.2022.12.022
28. Luo W, Tan J, Chen X, et al. Bioactive antiangiogenic lipid nanoparticles for inhibiting residual tumor growth after insufficient radiofrequency ablation. *ACS Appl Nano Mater*. 2024;7(11):12280–12289. doi:10.1021/acsanm.3c05540
29. Fang J, Tan J, Lin L, et al. Bioactive nanotherapeutic ultrasound contrast agent for concurrent breast cancer ultrasound imaging and treatment. *Adv Healthc Mater*. 2024;13(26):e2401436. doi:10.1002/adhm.202401436
30. Michaud M, Martins I, Sukkurwala AQ, et al. Autophagy-dependent anticancer immune responses induced by chemotherapeutic agents in mice. *Science*. 2011;334(6062):1573–1577. doi:10.1126/science.1208347
31. Obeid M, Tesniere A, Ghiringhelli F, et al. Calreticulin exposure dictates the immunogenicity of cancer cell death. *Nat Med*. 2007;13(1):54–61. doi:10.1038/nm1523
32. Apetoh L, Ghiringhelli F, Tesniere A, et al. Toll-like receptor 4-dependent contribution of the immune system to anticancer chemotherapy and radiotherapy. *Nat Med*. 2007;13(9):1050–1059. doi:10.1038/nm1622
33. Kroemer G, Galluzzi L, Kepp O, Zitvogel L. Immunogenic cell death in cancer therapy. *Annu Rev Immunol*. 2013;31(1):51–72. doi:10.1146/annurev-immunol-032712-100008
34. Huinen ZR, Huijbers EJM, van Beijnum JR, Nowak-Sliwinska P, Griffioen AW. Anti-angiogenic agents - overcoming tumour endothelial cell anergy and improving immunotherapy outcomes. *Nat Rev Clin Oncol*. 2021;18(8):527–540. doi:10.1038/s41571-021-00496-y
35. Amersfoort J, Eelen G, Carmeliet P. Immunomodulation by endothelial cells - partnering up with the immune system? *Nat Rev Immunol*. 2022;22(9):576–588. doi:10.1038/s41577-022-00694-4
36. Khan KA, Kerbel RS. Improving immunotherapy outcomes with anti-angiogenic treatments and vice versa. *Nat Rev Clin Oncol*. 2018;15(5):310–324. doi:10.1038/nrclinonc.2018.9
37. Kinoh H, Quader S, Shibasaki H, et al. Translational nanomedicine boosts anti-PD1 therapy to eradicate orthotopic PTEN-negative glioblastoma. *ACS Nano*. 2020;14(8):10127–10140. doi:10.1021/acsnano.0c03386
38. Li Y, Wu Y, Fang Z, et al. Dendritic nanomedicine with boronate bonds for augmented chemo-immunotherapy via synergistic modulation of tumor immune microenvironment. *Adv Mater*. 2024;36(2):e2307263. doi:10.1002/adma.202307263
39. Tang W, Chen Z, Zhang W, et al. The mechanisms of sorafenib resistance in hepatocellular carcinoma: theoretical basis and therapeutic aspects. *Signal Transduct Target Ther*. 2020;5(1):87. doi:10.1038/s41392-020-0187-x
40. Xia S, Pan Y, Liang Y, Xu J, Cai X. The microenvironmental and metabolic aspects of sorafenib resistance in hepatocellular carcinoma. *EBioMedicine*. 2020;51:102610. doi:10.1016/j.ebiom.2019.102610